JPE 16-1-6

http://dx.doi.org/10.6113/JPE.2016.16.1.48
ISSN(Print): 1598-2092 / ISSN(Online): 2093-4718

Demagnetization Detection for IPM-type BLDCMs According to Irreversible Demagnetization Patterns and Pole–Slot Coefficients

Dong-Hyeok Kang*, Hyung-Kyu Kim*, Jun-Kyu Park*, Seung-Ho Hyun*, and Jin Hur†

*Department of Electrical Engineering, University of Ulsan, Ulsan, Korea
†Department of Electrical Engineering, Incheon National University, Incheon, Korea

Abstract

This paper proposes a method for detecting irreversible demagnetization using the harmonic analysis of back electromotive force (BEMF) in interior permanent magnet-type brushless DC motors. First, demagnetization patterns, such as equality, inequality, and weighted demagnetizations, are defined and classified by considering the possibility of demagnetization resulting from motor operating characteristics. Second, an available diagnostic model for the harmonic analysis of BEMFs is defined according to pole–slot coefficients because the characteristics of BEMFs under demagnetization conditions are affected by the combination of poles and slots. Third, BEMFs and their harmonic components under normal and demagnetization conditions are analyzed through simulation and experiment to verify the proposed demagnetization detection technique.

Key words: Brushless DC motors, Demagnetization, Demagnetization patterns, Fault diagnosis, Permanent magnet motors, Pole–slot coefficient

I. INTRODUCTION

The stability and reliability of interior permanent magnet (IPM)-type brushless DC motors (BLDCMs) are verified in many studies and experiments. IPM-type BLDCMs are widely used in many applications because of their high performance per unit volume and excellent control. In particular, IPM-type BLDCMs are utilized as a core driving source in industries and electric vehicles because of their wide control range and high robustness. However, IPM-type BLDCMs also have potential risks, such as irreversible demagnetization, turn faults, and eccentricity faults [1]-[3]. Above all, irreversible demagnetization must be considered in BLDCMs. If these motors are continuously driven under irreversible demagnetization conditions, the residual flux densities of permanent magnets (PMs) decrease as demagnetizing regions increase owing to the overlap of inverse fluxes. Therefore, irreversible demagnetization faults must be detected.

A precise analysis of demagnetization is required for accuracy prediction and fault detection. Many studies have detected the demagnetization of PMs in various ways, such as by monitoring the zero-sequence voltage [4], using the harmonic components of linkage flux [5], and using the changes in i_d value [6].

The present study defines three types of demagnetization patterns for two types of BLDCM with different combinations of slots and poles. Flux linkage and back electromotive force (BEMF) waveforms are also analyzed with the finite element method (FEM) to confirm the changes in demagnetization characteristics according to newly defined demagnetization patterns. We then propose a novel technique for detecting irreversible demagnetization using the harmonic characteristics of BEMFs.

II. THREE TYPES OF DEMAGNETIZATION PATTERNS AND POLE–SLOT COEFFICIENTS

Irreversible demagnetization is generally induced by the increasing temperature of motors [7] and the sudden three-phase short circuit and overcurrent that are generated by

Manuscript received Sep. 16, 2015; accepted Dec. 12, 2015
Recommended for publication by Associate Editor Jung-Ik Ha.
†Corresponding Author: jinhur@inu.ac.kr
Tel: +82-32-835-0773, Fax: +82-32-835-8432, Incheon Nat'l University
*Dept. of Electrical Eng., University of Ulsan, Korea

inter-turn faults [8], [9]. The irreversible demagnetization of PMs is mainly caused by the armature reaction that occurs when the demand for starting torque is high [10].

Irreversible demagnetization can be classified into partial, symmetrical, and asymmetrical demagnetizations [11]-[13]. Previous studies have focused on the possibility of demagnetization in one magnet.

By contrast, the present study examines the possibility of irreversible demagnetization, which is characterized by different demagnetization ratios between N- and S-poles. All PMs tend to be demagnetized in the same degree, yet they are practically demagnetized in different degrees. For instance, all PMs are demagnetized in the same degree if the demagnetization is occurred by overcurrent resulting from overload.

An unbalanced magnetic field, which is caused by inter-turn faults or cracks from manufacturing defects, can lead to the unbalanced distribution of demagnetization for each pole [9]. Therefore, we classify irreversible demagnetization patterns into equality, inequality, and weighted demagnetization patterns [14].

We also determine the possibility of demagnetization according to the pole–slot coefficient (PSC). The demagnetization patterns are confirmed by the harmonic characteristics of BEMFs for two types of pole–slot combinations such as 6-pole 9-slot and 10-pole 12-slot models. Fig. 1 shows the pole configuration of 6- and 10-pole rotors.

A. Equality Demagnetization Pattern of PMs

The continuous overcurrent under overload conditions can lead to demagnetization. In this case, N- and S-poles have similar demagnetization ratios because of the balanced distribution of the air-gap magnetic field. Therefore, we consider this case as an equality demagnetization pattern. Fig. 2 shows a magnetization shape diagram that is constructed according to a demagnetization ratio of 50% and 70%. The magnetization shape resembles a lopsided step. In general, demagnetization does not occur evenly at the whole face of a PM because the magneto-motive force from the supplied power affects the nearby *q*-axis instead of the *d*-axis when the motor is in operation [9].

B. Inequality Demagnetization Pattern of PMs

Inter-turn fault causes an inverse air-gap magnetic field and lead to demagnetization [9]. In this case, N- and S-poles can be demagnetized in different ratios. Therefore, we consider this case as an inequality demagnetization pattern. Fig. 3 shows a magnetization shape diagram that is constructed according to different demagnetization ratios. The ratios of irreversible demagnetization patterns are N-pole 50%, S-pole 60% and N-pole 50%, S-pole 70%.

C. Weighted Demagnetization Pattern of PMs

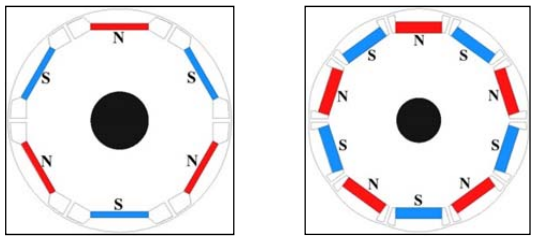

Fig. 1. Pole configuration for the utilized models.

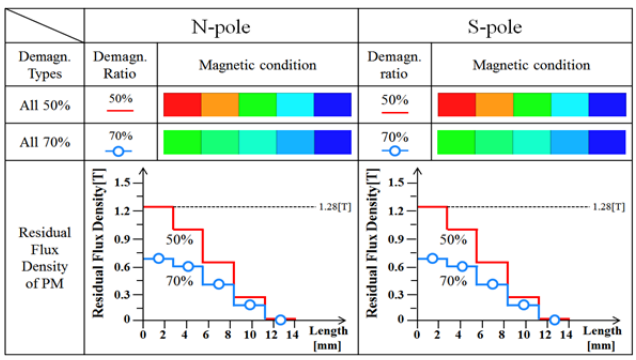

Fig. 2. Magnetization shape of equality demagnetization.

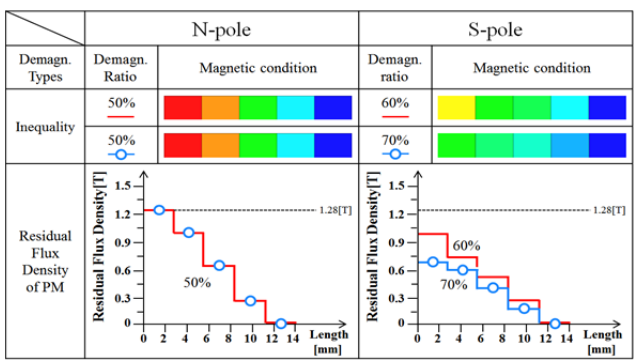

Fig. 3. Magnetization shape of inequality demagnetization.

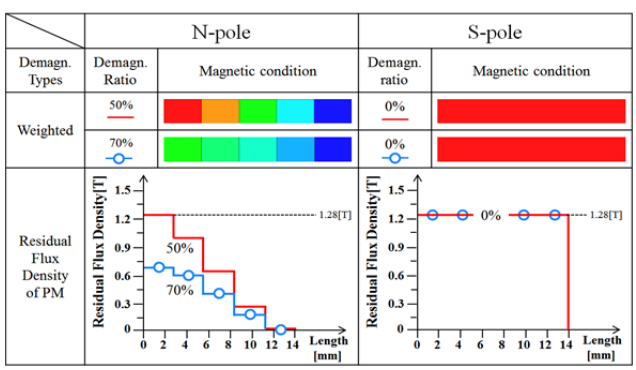

Fig. 4. Magnetization shape of weighted demagnetization.

Cracks and chips from manufacturing defects and physical damages can lead to demagnetization [15], [16]. In this case, only one of N-pole and S-pole can be demagnetized. For this reason, we consider this case as a weighted demagnetization pattern. Fig. 4 shows a magnetization shape diagram that is constructed according to the demagnetization ratio of a weighted demagnetization pattern. We apply demagnetization

only to the N-pole, which has demagnetization ratios of 50% and 70%.

D. Pole–Slot Coefficients

Before applying the demagnetization patterns, we select models according to the PSC shown in (1). A PSC can be classified as an integer or a non-integer. The analysis models are classified in terms of integer and non-integer ratios. When the rotor is rotating, an integer PSC indicates that all slots for one phase are successively affected by the N- or S-poles, respectively. By contrast, a non-integer PSC indicates that all slots for one phase are simultaneously affected by the N- and S-poles.

$$PSC = n \times \frac{p}{s} \tag{1}$$

where n is the number of phases, p is the pole pair, and s is the number of slots.

III. Simulation Results

In the case of the IPM-type BLDCM, the magnitude and waveform of the BEMF change when the PM is demagnetized because the BEMF obtains information on the structural elements of the motor, the number of poles, and the states of the PM. In other words, the BEMF shows the characteristics and status of the motor. Therefore, measuring BEMFs can help us understand the status of demagnetization. Moreover, measuring BEMFs is not a complex process. For this reason, BEMFs are considered as a detection parameter.

In the simulation analysis, we divided an irreversibly demagnetized PM into five pieces to achieve a lopsided step-shaped magnetization. In addition, we designated each of different the residual magnetic flux density values according to the demagnetization pattern in Table I.

As its most important feature, the proposed demagnetization detection method analyzes demagnetization according to PSCs and demagnetization patterns because demagnetization characteristics depend on the combination of poles and slots. Therefore, we analyzed the 6-pole 9-slot and 10-pole 12-slot models, which have different PSCs. The PSC of the 6-pole 9-slot model is an integer, whereas that of the 10-pole 12-slot model is a non-integer. Fig. 5 shows the 6-pole 9-slot and 10-pole 12-slot models. We performed a harmonic analysis of BEMFs under normal and demagnetization conditions to confirm the presence of additional harmonic components in each model.

A. 6-Pole 9-Slot Model

Fig. 5(a) shows the 6-pole 9-slot IPM-type BLDCM, Table II shows the specifications of the analysis models, and Fig. 6 shows the demagnetization patterns of 6-pole 9-slot IPM-type BLDCMs, such as equality, inequality, and weighted demagnetization patterns.

In the case of equality demagnetization, all PMs are demagnetized in equal degrees, as shown in Fig. 6(a). To confirm the demagnetization characteristics in different demagnetization ratios, we analyzed the type1 and type2 models and subsequently confirmed that the BEMF waveform has not distortions, as shown in Fig. 7(a).

Fig. 6(b) shows the inequality demagnetization, whereas Fig. 7(b) shows the BEMF waveform of inequality demagnetization. As a result of the inequality demagnetization pattern, type3 (N-pole 50% S-pole 60%) has more asymmetric BEMF waveforms than type4 (N-pole 50% S-pole 70%). In other words, inequality demagnetization has more asymmetric BEMF waveforms than equality demagnetization because of the large difference in the demagnetization ratios between the N- and S-poles. Therefore, the BEMF is distorted by the demagnetization ratio between the N- and S-poles.

TABLE I
Patterns and Ratios of Demagnetization

	Demagnetization ratio, [%]					
	Equality		Inequality		Weighted N	
	Type1	Type2	Type3	Type4	Type5	Type6
N-poles	50	70	50	50	50	70
S-poles	50	70	60	70	0	0

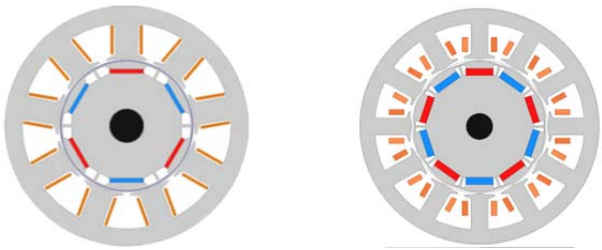

(a) 6-pole 9-slot. (b) 10-pole 12-slot.

Fig. 5. 6-pole 9-slot and 10-pole 12-slot IPM-type BLDCMs.

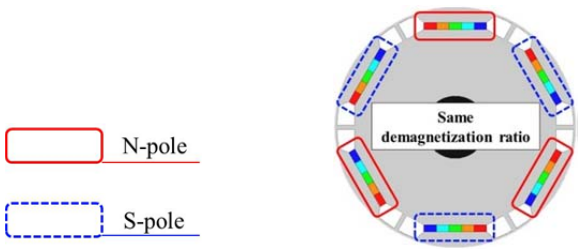

(a) Equality demagnetization.

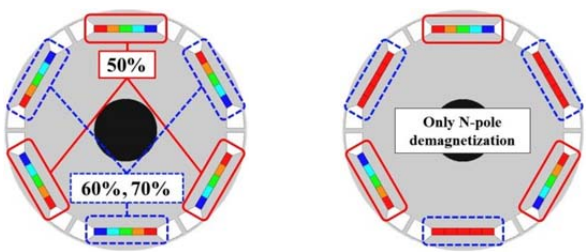

(b) Inequality demagnetization. (c) Weighted demagnetization.

Fig. 6. Demagnetization patterns of the 6-pole 9-slot model.

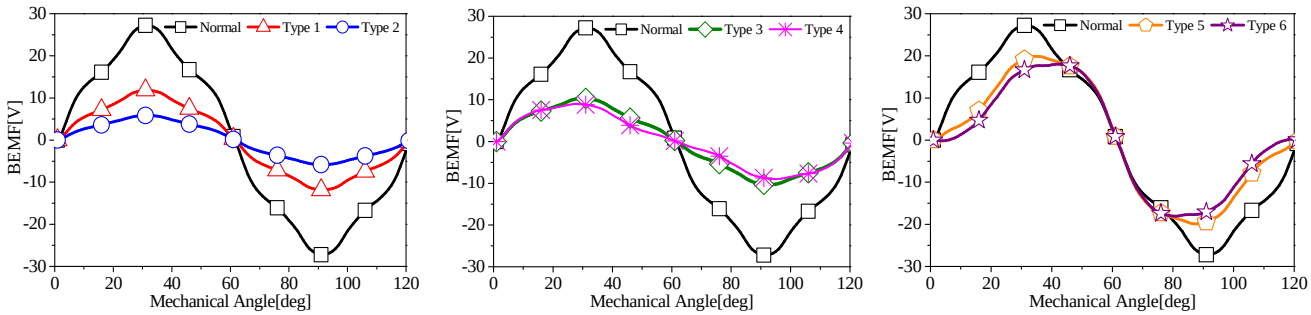

(a) Equality demagnetization. (b) Inequality demagnetization. (c) Weighted demagnetization.

Fig. 7. BEMF waveforms of the 6-pole 9-slot model.

TABLE II
SPECIFICATIONS OF THE 6-POLE 9-SLOT MODEL

Item	Value	Item	Value
Motor diameter [mm]	100	**Axial length [mm]**	40
Number of poles	6	**No. of slots**	9
Thickness of PM [mm]	1.5	**Br [T]**	1.28
No. of turns	72	**Speed [rpm]**	3300

TABLE III
SPECIFICATIONS OF THE 10-POLE 12-SLOT BLDCM

Item	Value	Item	Value
Motor diameter [mm]	90	**Axial length [mm]**	40
Number of poles	10	**No. of slots**	12
Thickness of PM [mm]	2.5	**Br [T]**	1.28
No. of turns	100	**Speed [rpm]**	3300

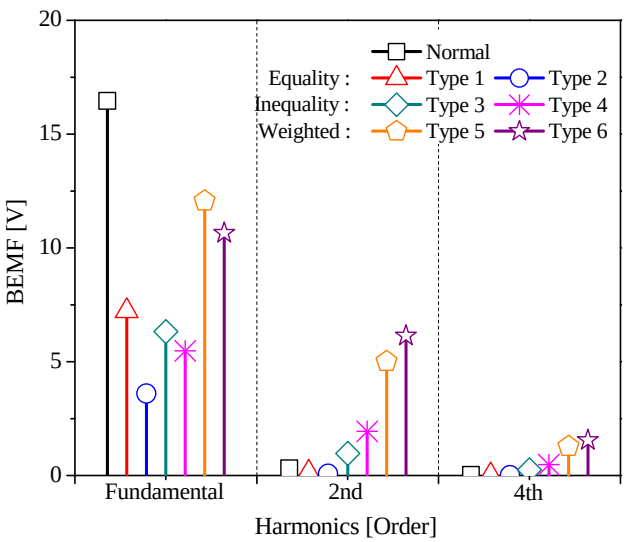

Fig. 8. Harmonic characteristics of the 6-pole 9-slot model.

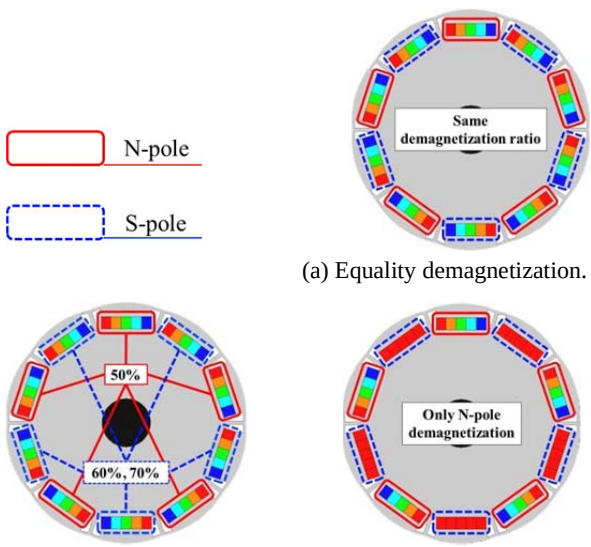

(a) Equality demagnetization.

(b) Inequality demagnetization. (c) Weighted demagnetization.

Fig. 9. Demagnetization patterns of the 10-pole 12-slot IPM-type BLDCM.

Fig. 6(c) shows the weighted demagnetization, whereas Fig. 7(c) shows the BEMF waveform of weighted demagnetization. The BEMF waveform of weighted demagnetization is more distorted than that of inequality demagnetization because the demagnetization ratio of the N- and S-poles is larger than inequality demagnetization.

Fig. 8 shows the BEMF harmonics analysis results for the three types of demagnetization patterns. In the case of equality demagnetization, only the fundamental harmonic size changes according to the demagnetization ratio. In addition, the second and fourth harmonics do not appear because the BEMF maintains the sinusoidal waveform. In the case of the inequality and weighted demagnetization patterns, the fundamental harmonic size is reduced in proportion to the demagnetization ratio. However, the second and fourth harmonics have comparatively large values unlike the equality demagnetization pattern. When the motor is in operation, the second and fourth harmonics of the BEMF are formed because of the differences in the flux linkages of the N- and S-poles.

B. 10-Pole 12-Slot Model

Fig. 5(b) shows the 10-pole 12-slot IPM-type BLDCM with a fractional slot characteristic unlike the 6-pole 9-slot

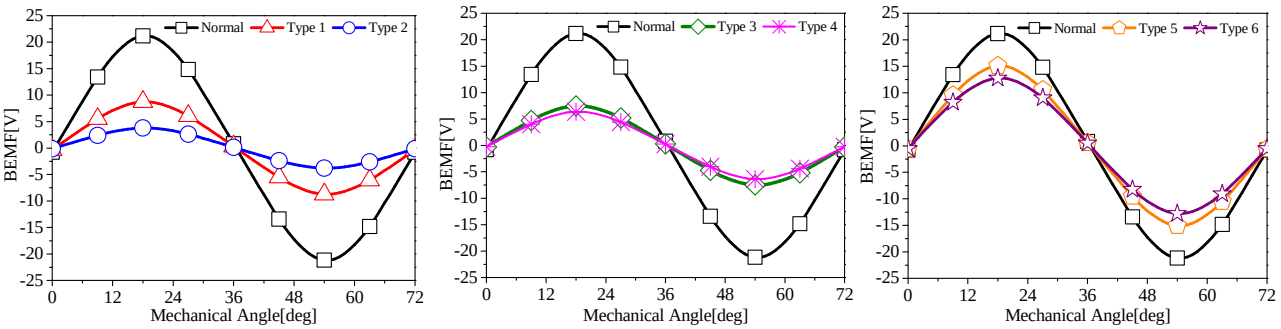

(a) Equality demagnetization. (b) Inequality demagnetization. (c) Weighted demagnetization.

Fig. 10. BEMF waveforms of the 10-pole 12-slot IPM-type BLDCM.

model. This model also has a different pole–slot combination ratio. This model was selected to confirm the BEMF harmonic characteristics of another model with a different pole–slot combination ratio. Table III shows the specifications of the 10-pole 12-slot IPM-type BLDCM, whereas Fig. 9 shows the conceptual figure of this model when applied to equality, inequality, and weighted demagnetization patterns.

Fig. 10(a) shows the BEMF analysis results in the case of equality demagnetization. The BEMF waveform is symmetrical because the demagnetization ratios of the N- and S-poles are the same. Therefore, the waveform is not distorted.

Fig. 10(b) shows the BEMF waveforms in the case of inequality demagnetization. In contrast to that in the 6-pole 9-slot model, the BEMF waveform in the current model is not distorted. Fig. 10(c) shows the BEMF analysis results for the weighted demagnetization pattern. Similar to that of the 6-pole 9-slot model, the magnitude of the waveform of the current model is decreased. Although the 6-pole 9-slot model shows the most distorted demagnetization pattern, the BEMF of the 10-pole 12-slot model is not distorted.

Fig. 11 shows the BEMF harmonics analysis results of the 10-pole 12-slot model according to the demagnetization patterns. The second and fourth harmonics have extremely small values in the 10-pole 12-slot model because the N-poles of the PMs in the integer PSC model are all located in the slot of one phase. By contrast, when the N-pole of the non-integer PSC model is located in the slot of one phase, the S-pole is located in another slot of the same phase. That is, in the case of the integer PSC model (6-pole 9-slot), only the N-pole affects the A-phase in the rotor position with the maximum linkage flux. In the case of the non-integer PSC model (10-pole 12-slot), the pole pair affects the A-phase in the rotor position with the maximum linkage flux, as shown in Fig. 12. The equivalent diagrams of the two models are shown in Fig. 13.

We confirmed the BEMF harmonic characteristics by analyzing various IPM-type BLDCMs. These characteristics can be used for irreversible demagnetization detection under integer PSC models.

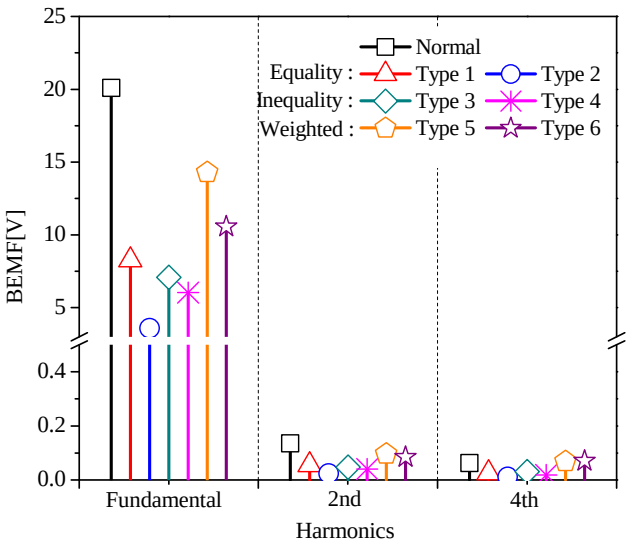

Fig. 11. Harmonic characteristics of the 10-pole 12-slot model.

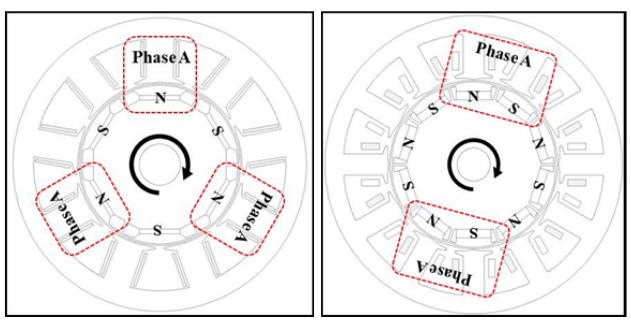

(a) 6-pole 9-slot model (PSC = 1). (b) 10-pole 12-slot model (PSC = 1.25).

Fig. 12. Phase A of the 6-pole 9-slot and 10-pole 12-slot models.

IV. Experimental Results

By analyzing the type5 model for different N- and S-pole demagnetization ratios, we confirmed that the presence of second and fourth harmonics allowed for the irreversible demagnetization detection of the PM. Therefore, we performed an experiment with the test motors to verify if the proposed detection technique could be used in BLDCM applications.

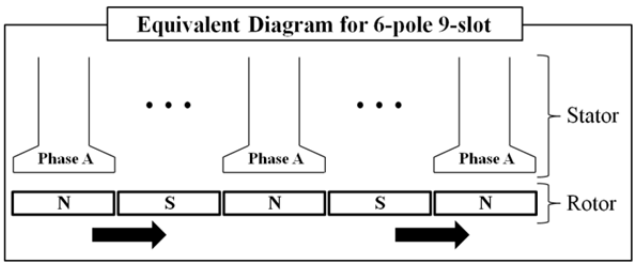

(a) 6-pole 9-slot model.

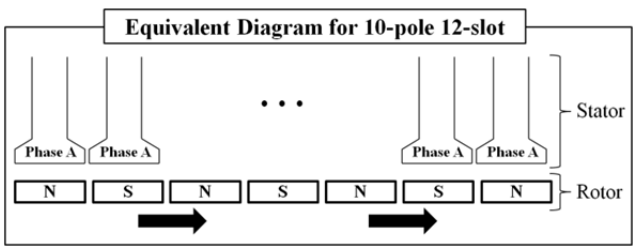

(b) 10-pole 12-slot model.

Fig. 13. Equivalent diagrams for the 6-pole 9-slot and 10-pole 12-slot models.

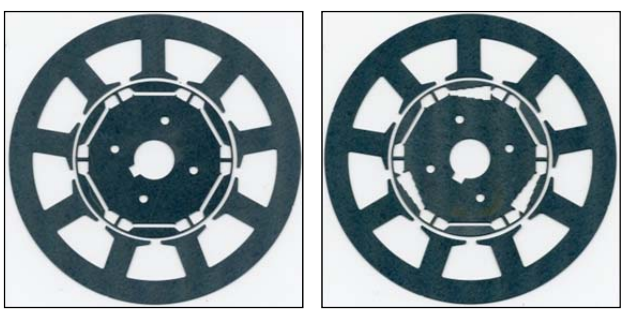

(a) Normal (non-demagnetization). (b) Test (type5).

Fig. 14. Normal and test motors of the 6-pole 9-slot model for the experiment.

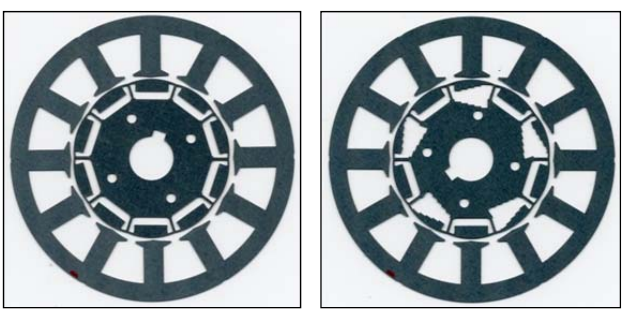

(a) Normal (non-demagnetization). (b) Test (type5).

Fig. 15. Normal and test motors of the 10-pole 12-slot model for the experiment.

The experiment was performed under the same condition as in the simulation with 3,300 rpm. Figs. 14(a) and 15(a) show the normal condition models used in the experiment. The cross sections of the test motors are shown in Figs. 14(b) and 15(b). Because the test motors are small and it is very difficult for its demagnetized condition to be realized using the division method of the PM, the demagnetized magnet

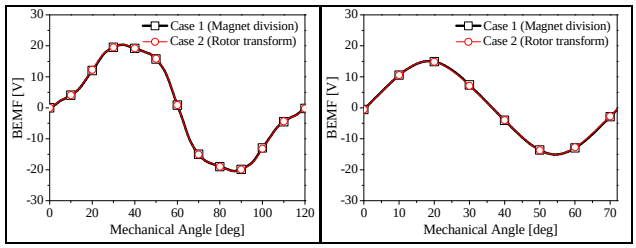

(a) 6-pole 9-slot model. (b) 10-pole 12-slot model.

Fig. 16. BEMF simulation results for the magnet division and rotor transform models of type5.

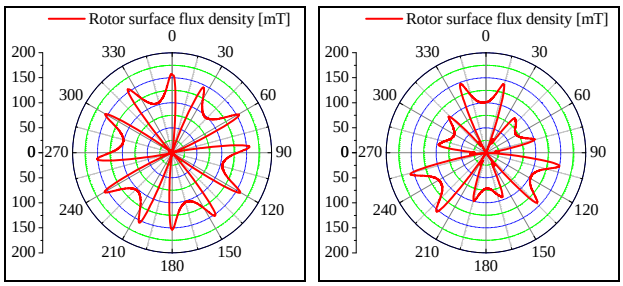

(a) Normal. (b) Test (type5).

Fig. 17. Surface magnetic flux density for the 6-pole 9-slot model.

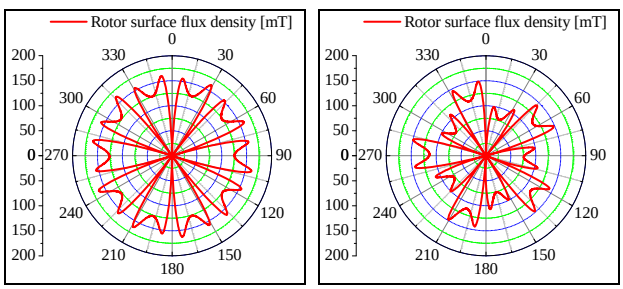

(a) Normal. (b) Test (type5).

Fig. 18. Surface magnetic flux density for the 10-pole 12-slot model.

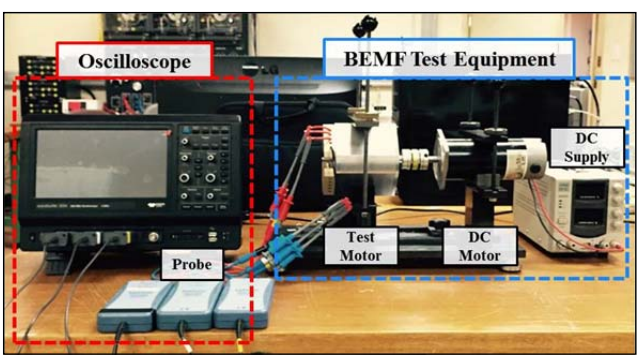

Fig. 19. Experimental equipment.

portion is fabricated in air, and has a step shape in order to realize the type 5 condition. We compared the simulation results of the rotor transformation and magnet division models to justify the use of the rotor transformation model. The results are shown in Figs. 16(a) and (b). The BEMF of the existing magnet division and that of the rotor-core

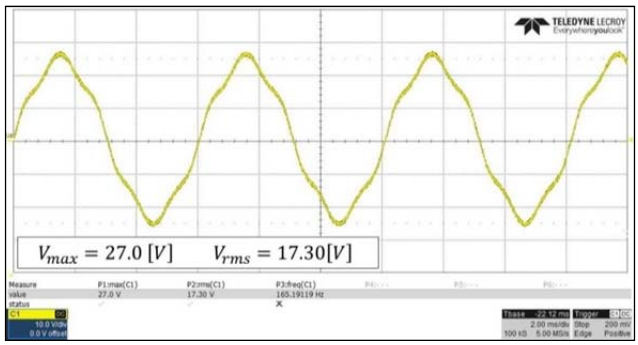

(a) Normal (non-demagnetization) condition.

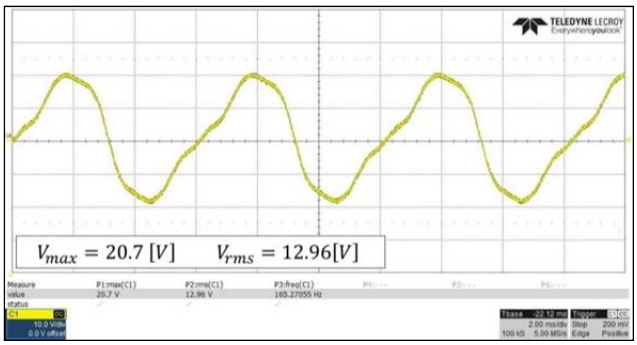

(b) Type5 (N-pole 50% demagnetization) condition.

Fig. 20. Experiment results of the BEMF for the 6-pole 9-slot model.

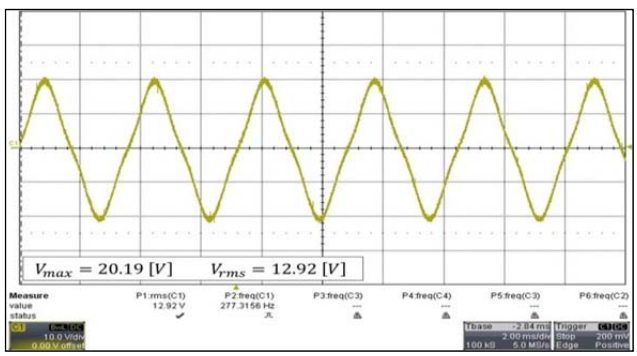

(a) Normal (non-demagnetization) condition.

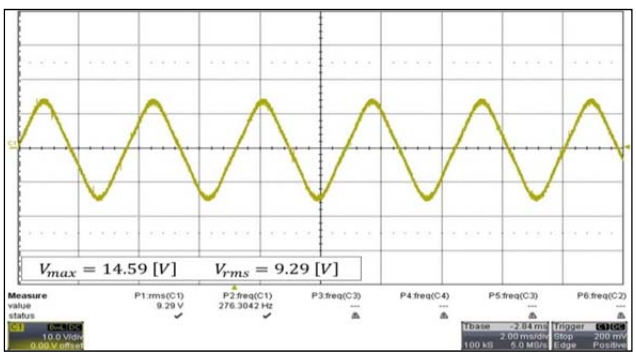

(b) Type5 (N-pole 50% demagnetization) condition.

Fig. 21. Experiment results of the BEMF for the 10-pole 12-slot model.

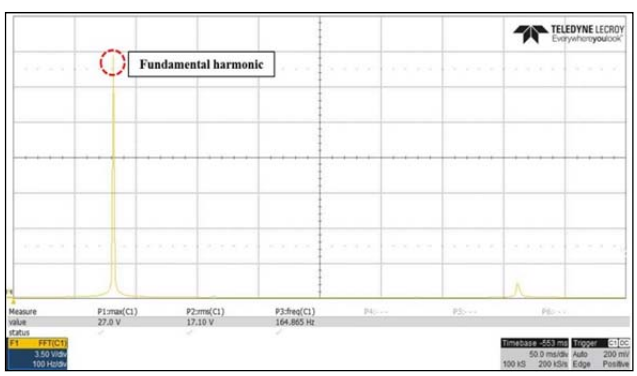

(a) Normal (non-demagnetization) condition.

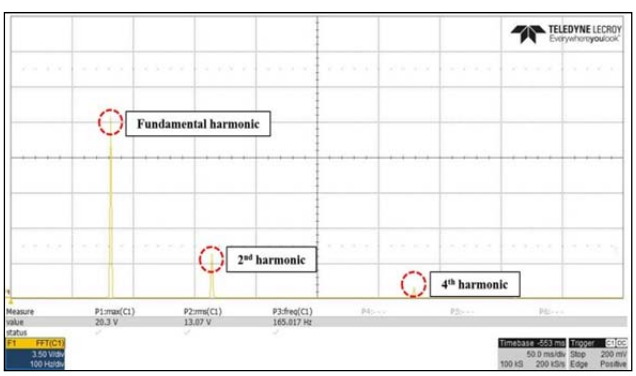

(b) Type5 (N-pole 50% demagnetization) condition.

Fig. 22. Experiment results of the harmonic characteristics for the 6-pole 9-slot model.

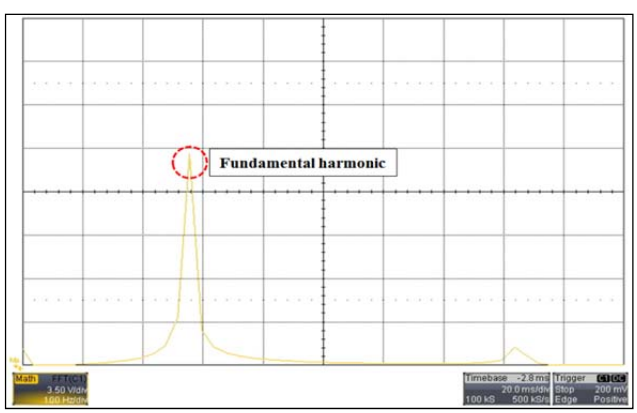

(a) Normal (non-demagnetization) condition.

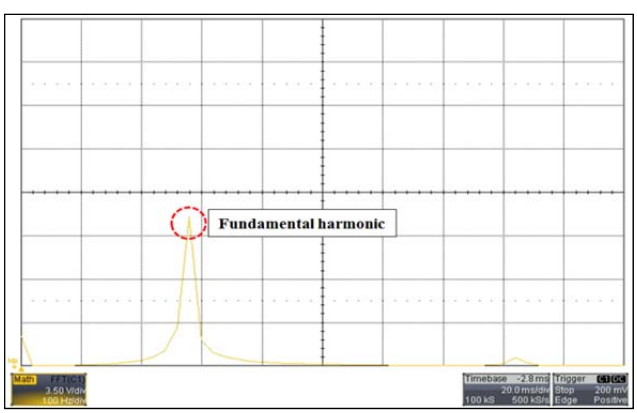

(b) Type5 (N-pole 50% demagnetization) condition.

Fig. 23. Experiment results of the harmonic characteristics for the 10-pole 12-slot model.

transformation models in the experiment are highly similar.

Figs. 17 and 18 show the rotor surface magnetic flux densities for the normal and demagnetized condition models. The magnetic flux density of the N-pole is smaller than that of the S-pole on the rotor surface. Fig. 19 shows the experiment equipment used to measure and analyze the BEMF and harmonic characteristics of the two models (6-pole 9-slot and 10-pole 12-slot).

A. BEMF Results

Figs. 20 and 21 show the experimental results for the BEMF of the normal condition and test motors (type5). Figs. 20(a) and 21(a) show the BEMF results of the normal condition motor for the 6-pole 9-slot and 10-pole 12-slot models, respectively. The BEMF result for the normal condition motor is not biased to one side because the positive and negative areas are symmetric. However, the BEMF of the 6-pole 9-slot test motor exhibits an asymmetric waveform in the positive and negative areas, as shown in Fig. 20(b). By contrast, the BEMF of the 10-pole 12-slot test motor is not biased to one side, as shown in Fig. 21(b), because the 6-pole 9-slot model has an integer PSC, whereas the 10-pole 12-slot model has a non-integer PSC.

B. Harmonic Characteristics

Figs. 22 and 23 show the fast Fourier transform (FFT) analysis results of the BEMF for the normal condition and test motors. Similar to the simulation results, the harmonic component does not appear under the normal condition motor, as shown in Figs. 22(a) and 23(a). By contrast, the second and fourth harmonic components are only observed under the demagnetized 6-pole 9-slot model, as shown in Fig. 22(b). However, the second and fourth harmonics are not observed under the demagnetized 10-pole 12-slot model, as shown in Fig. 23(b). These results are observed when the BEMF is biased to one side, which indicates that the N- and S-poles have different demagnetization ratios under the integer PSC condition. Therefore, demagnetization conditions can easily be detected by using the second and fourth harmonic characteristics of the BEMF for the integer PSC model.

V. CONCLUSION

In this study, we proposed a novel detection technique for the irreversible demagnetization of IPM-type BLDCMs. First, we classified irreversible demagnetization patterns into equality, inequality, and weighted demagnetization patterns. Second, we defined two models according to PSCs. Third, we confirmed the occurrence of the second and fourth harmonic components of the BEMF through FFT analysis. Specifically, we only observed inequality and weighted demagnetization patterns in the second and fourth harmonic components of the integer PSC model. In conclusion, the integer PSC model can detect an irreversible demagnetization condition via a harmonic component analysis of BEMFs.

ACKNOWLEDGMENT

This work was financially supported by the Energy Efficiency and Resources of the Korea Institute of Energy Technology Evaluation and Planning grant funded by the Korea Government Ministry of Knowledge Economy (No. 20122010100130) and the Ministry of Science, ICT, and Future Planning of Korea under the IITP-supervised C-ITRC IITP-2015-H8601-15-1005.

REFERENCES

[1] D. J. McFarland and T. M. Jahns, “Investigation of the rotor demagnetization characteristics of interior PM synchronous machines during fault conditions,” *IEEE. Trans. Ind. Applicat.*, Vol. 50, No. 4, pp. 2768-2775, Jul./Aug. 2014.

[2] A. Sarikhani and O. A. Mohammed, “Inter-turn fault detection in PM synchronous machines by physics-based back electromotive force estimation,” *IEEE. Trans. Ind. Electron.*, Vol. 60, No. 8, pp. 3472-3484, Aug. 2013.

[3] S. Rajagopalan, J. M. Aller, J. A. Restrepo, T. G. Habetler, and R. G. Harley, “Analytic-wavelet-ridge-based detection of dynamic eccentricity in brushless direct current (BLDC) motors functioning under dynamic operating conditions,” *IEEE. Trans. Ind. Electron.*, Vol. 54, No. 3, pp. 1410-1419, Jun. 2007.

[4] J. Urresty, J.-R. Riba Ruiz, M. Delgado, and L. Romeral, “Detection of demagnetization faults in surface-mounted permanent magnet synchronous motors by means of the zero-sequence voltage component,” *IEEE. Trans. Energy Convers.*, Vol. 27, No. 1, pp. 42-51, Mar. 2012.

[5] D. Torregrossa, A. Khoobroo, and B. Fahimi, “Prediction of acoustic noise and torque pulsation in PM synchronous machine with static eccentricity and partial demagnetization using field reconstruction method,” *IEEE Trans. Ind. Electron.*, Vol. 59, No. 2, pp. 934-944, Feb. 2012.

[6] J. M. Hong, S. U. Park, D. S. Hyun, T. J. Kang, S. B. Lee, and C. Kral, “Detection and classification of rotor demagnetization and eccentricity faults for PM synchronous motors,” *IEEE. Trans. Ind. Applicat.*, Vol. 48, No. 3, pp. 923-932, May/Jun. 2012.

[7] P. Zhou, D. Lin, Y. Xiao, N. Lambert, and M. A. Rahman, “Temperature-dependent demagnetization model of permanent magnets for finite element analysis,” *IEEE. Trans. Magn.*, Vol. 48, No.2, pp. 1031-1034, Feb. 2012.

[8] T. Hosoi, H. Watanabe, K. Shima, T. Fukami, R. Hanaoka, and S. Takata, “Demagnetization analysis of additional permanent magnets in salient-pole synchronous machines with damper bars under sudden short circuits,” *IEEE. Trans. Ind. Electron.*, Vol. 59, No. 6, pp. 2448-2456, Jun. 2012.

[9] Y. S. Lee, K. T. Kim, and J. Hur, “Finite-element analysis of the demagnetization of IPM-type BLDC motor with stator turn fault,” *IEEE. Trans. Magn.*, Vol. 50, No. 2, Feb. 2014.

[10] A. G. Espinosa, J. A. Rosero, J. Cusido, L. Romeral, and J. A. Ortega, “Fault detection by means of Hilbert-Huang transform of the stator current in a PMSM with

demagnetization," *IEEE. Trans. Energy Convers.*, Vol. 25, No. 2, pp. 312-318, Jun. 2010.
[11] K. C. Kim, K. S. Kim, H. J. Kim, and J. Lee, "Demagnetization analysis of permanent magnets according to rotor types of interior permanent magnet synchronous motor," *IEEE. Trans. Magn.*, Vol. 45, No. 6, pp. 2799-2802, Jun. 2009.
[12] L. Silong, L. Yingjie, and B. Sarlioglu, "Partial Irreversible Demagnetization assessment of flux-switching permanent magnet machine using ferrite permanent magnet material," *IEEE. Trans. Magn.*, Vol. 51, No. 7, Feb. 2015.
[13] V. I. Patel, J. Wang, and S. S. Nair, "Demagnetization assessment of fractional-slot and distributed wound 6-phase permanent magnet machines," *IEEE. Trans. Magn.*, Vol. 51, No. 6, Dec. 2014.
[14] D. H. Kang, J. K. Park, S. H. Hyun, and J. Hur, "BEMF characteristic analysis of IPM type motor according to demagnetization pattern of permanent magnet," in *proc. International Conference on Power Electronics and ECCE Asia (ICPE-ECCE Asia)*, pp. 714-721, 2015.
[15] J. A. Farooq, A. Djerdir, and A. Miraoui, "Analytical modeling approach to detect magnet defects in permanent-magnet brushless motors," *IEEE. Trans. Magn.*, Vol. 44, No. 12, pp. 4599-4604, Dec. 2008.
[16] S. Rajagopalan, W. Roux, T. G. Habeltler, and R. G. Harley, "Dynamic eccentricity and demagnetization rotor magnet detection in trapezoidal flux (Brushless DC) motors operating under different load conditions," *IEEE. Trans. Power Electron.*, Vol. 22, No. 5, pp. 2061-2069, Sep. 2007.

Dong-Hyeok Kang was born in Changwon, Korea, in 1990. He received his bachelor's degree in electrical engineering from the University of Ulsan, Ulsan, Korea, in 2015. Since 2015, he has been pursuing his master's degree in electrical engineering at the University of Ulsan, Ulsan, Korea. His current research interests include motor design and motor fault diagnosis.

Hyung-Kyu Kim received his bachelor's and master's degrees in electrical engineering from the University of Ulsan, Ulsan, Korea, in 2009 and 2011, respectively. From 2011 to 2013, he worked as a senior researcher of the Electric & Electronic Research Division of the Korea Marine Equipment Research Institute, Busan, Korea. Since 2014, he has been pursuing his doctor's degree in electrical engineering at the University of Ulsan, Ulsan, Korea. His current research interests include motor design, irreversible demagnetization analysis, and motor fault diagnosis.

Jun-Kyu Park was born in Busan, Korea, in 1986. He received his bachelor's and master's degrees in electrical engineering from the University of Ulsan, Ulsan, Korea, in 2011 and 2013, respectively. Since 2014, he has been pursuing his doctor's degree in electrical engineering at the University of Ulsan, Ulsan, Korea. His current research interests include motor design, motor vibration analysis, and motor fault diagnosis.

Seung-Ho Hyun received his bachelor's, master's, and doctor's degrees in electrical engineering from Seoul National University, Korea, in 1991, 1993, and 1996, respectively. From 1996 to 2002, he served as the manager of the High Speed Rail Systems Engineering Team of the Korea Railroad Research Institute. He also worked as a research professor in Myongji University from 2002 to 2004. He is currently working as an associate professor in the School of Electrical Engineering, University of Ulsan, Korea. His major research fields include power system control, protection, and renewable energy.

Jin Hur received his doctor's degree in electrical engineering from the Hanyang University, Seoul, Korea, in 1999. From 1999 to 2000, he served as a postdoctoral research associate in the Department of Electric Engineering, Texas A&M University, College Station, TX. From 2000 to 2001, he worked as a research professor of electrical engineering for BK21 projects in Hanyang University. From 2002 to 2007, he served as the director of the Intelligent Mechatronics Research Center, Korea Electronics Technology Institute, Puchon, Korea, where he developed special electric machines and systems. From 2008 to August 2015, he served as an associate professor in the School of Electric Engineering, University of Ulsan, Ulsan, Korea. Since August 2015, he has been working as a professor in the Department of Electrical Engineering, Incheon National University, Incheon, Korea. He has published over 140 articles on electric machine design, analysis and control, and power electronics. He has one granted/pending US patent and 20 granted/pending Korean patents. His current research interests include high-performance electrical machines, modeling, drives, new concept actuators for special purposes, and numerical analysis of electromagnetic fields. Dr. Hur is also working as an associate editor for IEEE Transaction on Power Electronics.